# NUMERICAL CALCULATION OF HIGH-ORDER, CONSTRAINED INNER LOOP TRANSFER FUNCTIONS

Roberto Celi
Department of Aerospace Engineering,
University of Maryland,
College Park, Maryland 20742, USA.

## Abstract

The paper presents the derivation of three techniques for the numerical calculation of multi-loop transfer functions. Because these techniques do not require symbolic manipulations, they allow the introduction of rotor dynamics and other higher-order effects in the calculation of the transfer functions. The techniques are applied to the study of the roll dynamics of a hingeless rotor helicopter with the pitch and yaw response eliminated by assuming infinitely tight feedback loop. Both straight and turning flight conditions are considered. The combination of perfect pilot regulation of off-axis response and low frequency rotor modes can have repercussion on handling qualities. Significant bandwidth changes can be observed, and the constrained system typically switches from phase- to gain-limited. However, the bandwidth changes are caused by the nonlinearity of the gain and phase curves around the phase crossover frequency, therefore, their practical significance remains to be determined. The combination of perfect pilot regulation of off-axis response and low frequency rotor modes can negatively affect aeroelastic stability. For the configuration analyzed, the damping of the regressive lag mode drops substantially with perfect pitch and yaw regulation, both in straight and in turning flight. The possibility of destabilizing pilot-rotor coupling appears to exist. The previous conclusions are valid for a "perfect" regulation obtained assuming infinitely high gains in the off-axis response feedback loops. While this assumption is convenient and simple, it should be critically examined for every configuration. Most of the effects of perfect regulation on the bandwidth occur for gains so high that they cannot be considered completely realistic. This is generally also true for the effects on aeroelastic stability, but some symptoms of pilot-rotor coupling do appear for realistic values of gains, so the phenomenon merits further study.

Professor, Alfred Gessow Rotorcraft Center; e-mail: celi@eng.umd.edu.
Paper presented at the 30th European Rotorcraft Forum, Marseilles, France, September 14-16, 2004.

## Notation

| | |
|---|---|
| $A_{SS}, B_{SS}$ | State and control matrix of system in state-space form |
| $A(s), B(s)$ | State and control matrix of system in Laplace transformed form |
| $n_T$ | Load factor in a turn |
| $N^{\phi}_{\delta_{lat}}$ | Example of numerator |
| $N^{\phi}_{\delta_{lat}\theta}$ | Example of coupling numerator |
| $N^{\phi}_{\delta_{lat}\delta_{lon}}$ | Example of type-two coupling numerator |
| $N^{\phi}_{\delta_{lat}\delta_{lon}\delta_{ped}}$ | |
| $\mathbf{u}$ | Control vector |
| $V$ | Flight speed |
| $\mathbf{x}$ | State vector |
| $Y_{\theta}$ | Pilot transfer function in closure of pitch attitude loop |
| $Y_{\psi}$ | Pilot transfer function in closure of yaw attitude loop |
| $\gamma$ | Flight path angle |
| $\delta_{lat}, \delta_{lon}, \delta_{ped}$ | Lateral, longitudinal, and pedal input |
| $\Delta$ | Characteristic polynomial of system matrix $A(s)$ |
| $\theta_{1c}$ | Lateral cyclic pitch |
| $\mu$ | Advance ratio |
| $\phi, \theta, \psi$ | Roll, pitch, and yaw angles |
| $\omega_{180}$ | Phase crossover frequency |

## Introduction

The response of a helicopter to pilot inputs is different if some degrees of freedom are constrained or prescribed. For example, if the pilot maneuvers in one degree of freedom while trying to constrain the others, the handling qualities characteristics of the helicopter can change, and pilot-induced instabilities may even ensue. It is also possible that the aeromechanic stability of lower frequency rotor modes can be affected by pilot loop closures. A detailed discussion of these phenomena can be found in the textbook by Padfield [1].

A key ingredient for a better understanding of constrained helicopter dynamics is the availability of adequate analysis tools, especially when one wishes to include the effects of rotor dynamics through simulation models of realistic complexity. The effect on helicopter dynamics of constraining degrees of freedom can be modeled in three main ways.

The first is to set to zero the portions of the model corresponding to the constrained degrees of freedom. This is the simplest technique, but it tends to be inaccurate, especially for highly coupled systems like helicopters with hingeless or bearingless rotors.

The second is the quasi-static reduction of the constrained degrees of freedom. Consider the model in linearized form, and partition the state vector $\mathbf{x}$ into a portion $\mathbf{x}_R$ to be retained and a portion $\mathbf{x}_D$ to be removed:

$$\left\{ \begin{array}{c} \dot{\mathbf{x}}_R \\ \dot{\mathbf{x}}_D \end{array} \right\} = \left[ \begin{array}{cc} A_{RR} & A_{RD} \\ A_{DR} & A_{DD} \end{array} \right] \left\{ \begin{array}{c} \mathbf{x}_R \\ \mathbf{x}_D \end{array} \right\} + \left[ \begin{array}{c} B_R \\ B_D \end{array} \right] \mathbf{u} \quad (1)$$

Then, if it can be assumed that the states $\mathbf{x}_D$ are infinitely fast, so that one can write $\dot{\mathbf{x}}_D = 0$, then the lower partitions of Eq. (1) can be solved for $\mathbf{x}_D$, and the solution substituted back in the upper partitions. This results in the reduced order model

$$\dot{\mathbf{x}}_R = A_{red}\mathbf{x}_R + B_{red}\mathbf{u} \quad (2)$$

with

$$A_{red} = A_{RR} - A_{RD}A_{DD}^{-1}A_{DR} \quad (3)$$

$$B_{red} = B_R - A_{RD}A_{DD}^{-1}B_D \quad (4)$$

This is a widely used technique that, however, is acceptable only if there is a clear frequency separation between the dynamics to be left free and the dynamics to be constrained [1]. This assumption may be inaccurate for configurations with highly coupled rotor-body modes such as coupled roll-regressive flap or -regressive lag modes.

The third is the derivation of multi-loop transfer functions, and the use of coupling numerator theory [2]. The key derivations and definitions of this theory are briefly summarized in the Appendix. This approach is the most rigorous, and it has been used in many helicopter related studies. For example, in Ref. [4] it is used for fundamental studies of helicopter flight dynamics with the pilot in the loop. In Ref. [5], it is used in the context of the design of digital flight control systems. In Ref. [6] coupling numerators are used to determine ideal crossfeeds in a flight control system designed using quantitative feedback theory. Unfortunately, the theory has proved impractical for higher order systems, such as coupled rotor-fuselage models, because it requires the symbolic calculation of determinants. This limits the practical size of the systems that can be analyzed.

The general objective of this paper is to improve the fundamental understanding of helicopter dynamics in constrained conditions, especially in the area at the intersection of the handling qualities and rotor dynamics fields, i.e., the closed loop behavior of the coupled rotor-fuselage system when the loop is closed by the pilot. More specifically, the objectives of the paper are:

1. To present the development of three techniques to obtain multi-loop transfer functions numerically, rather than symbolically. Therefore, these techniques can be conveniently applied to helicopter mathematical models of arbitrary complexity.

2. To study the effect of completely constraining some rigid body degrees of freedom on selected handling qualities characteristics, such as bandwidth.

3. To study the effect of pilot dynamics on the aeromechanic stability of low frequency rotor modes, and explore the possibility of pilot-rotor coupling.

## Inner loop model

Although the techniques developed in this paper are quite general, they will be described through their application to a specific example, namely, the extraction of inner loop transfer functions. The corresponding block diagram is shown in Figure 1. Recall that a normal helicopter piloting technique can be assumed to be separated into a higher frequency control of roll, pitch, and yaw attitudes through lateral cyclic, longitudinal cyclic, and pedal, respectively (the "inner loops"), and a lower frequency control of longitudinal position or velocity, lateral position or velocity, and altitude or flight path angle, through commanded pitch attitude, commanded roll attitude, and collective stick (the "outer loops") [4]. More specifically, Fig. 1 depicts the block diagram appropriate for the derivation of the transfer function from lateral cyclic $\delta_{lat}$ to roll angle $\phi$, while the pilot closes the off-axis pitch and yaw attitude loops with transfer functions $Y_\theta$ and $Y_\psi$, to achieve desired (or commanded) pitch and yaw angles $\theta_C$ and $\psi_C$. For the present study, $\theta_C = \psi_C = 0$, i.e., the pilot is trying to cancel the off-axis response to lateral cyclic.

The corresponding following open-loop roll transfer function is:

$$\left. \frac{\phi(s)}{\delta_{lat}(s)} \right|_{\begin{array}{l} \theta \rightarrow \delta_{lon} \\ \psi \rightarrow \delta_{ped} \end{array}} \quad (5)$$

where the notation indicates that the pilot closes the pitch loop with longitudinal cyclic command ($\phi \rightarrow \delta_{lat}$) and the yaw loop with pedal command ($\psi \rightarrow \delta_{ped}$).

Using coupling numerator theory [2], the transfer function is given by [4]

$$\left. \frac{\phi}{\delta_{lat}} \right|_{\begin{array}{l} \theta \rightarrow \delta_{lon} \\ \psi \rightarrow \delta_{ped} \end{array}} = \frac{N^{\phi}_{\delta_{lat}} + Y_\theta N^{\phi\ \theta}_{\delta_{lat}\delta_{lon}} + Y_\psi N^{\phi\ \psi}_{\delta_{lat}\delta_{ped}} + Y_\theta Y_\psi N^{\phi\ \theta\ \psi}_{\delta_{lat}\delta_{lon}\delta_{ped}}}{\Delta + Y_\theta N^{\theta}_{\delta_{lon}} + Y_\psi N^{\psi}_{\delta_{ped}} + Y_\theta Y_\psi N^{\theta\ \psi}_{\delta_{lon}\delta_{ped}}} \quad (6)$$

The key derivations and definitions of multi-loop transfer functions using coupling numerator theory are briefly summarized in the Appendix. In Eq. (6), the $N$ terms, and $Y_\theta$ and $Y_\psi$ are generally all functions of $s$. The specific forms of $Y_\theta$ and $Y_\psi$ depend on the individual pilot, but guidance on their general characteristics (e.g., amount of equalization, gain, etc.) can be obtained from a mathematical theory of human pilot modeling [3].

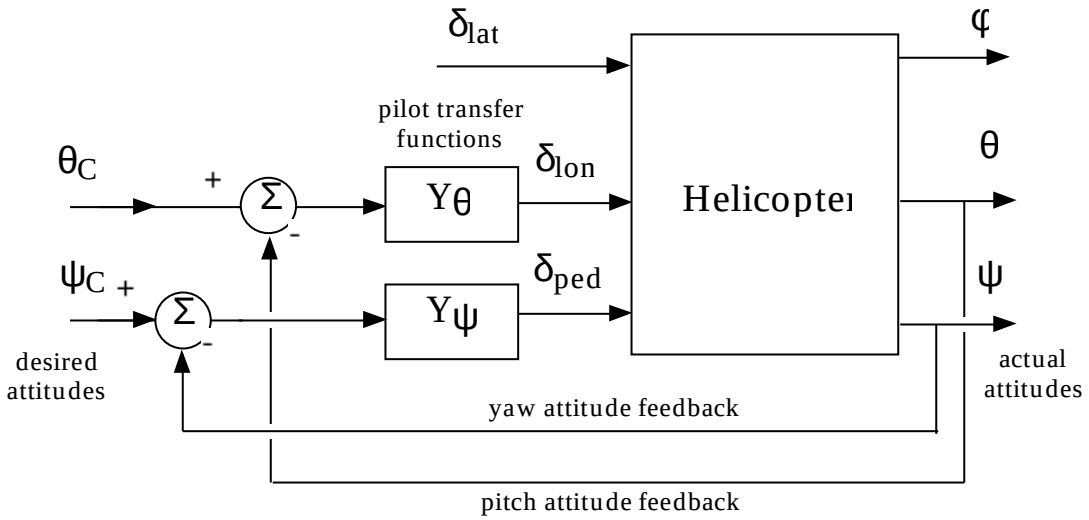


Figure 1: Block diagram for $\phi(s)/\delta_{lat}(s)$ inner loop analysis; open loop roll with pitch and yaw regulation.

If there is no attempt to regulate $\theta$ and $\psi$ (by the pilot or by a flight control system), then $Y_\theta = Y_\psi = 0$ and the transfer function, Eq. (6), becomes simply:

$$\frac{\phi(s)}{\delta_{lat}(s)} = \frac{N^{\phi}_{\delta_{lat}}}{\Delta} \tag{7}$$

which is the open loop roll transfer function. If both the pitch and the yaw feedback loops are assumed to be infinitely tight, then both $\theta$ and $\psi$ are zero, and the transfer function Eq. (6) becomes

$$\left.\frac{\phi(s)}{\delta_{lat}(s)}\right|_{\substack{\theta \to \delta_{lon} \\ \psi \to \delta_{ped}}} \quad \to$$

$$\to \lim_{\substack{Y_\theta \to \infty \\ Y_\psi \to \infty}} \left.\frac{\phi(s)}{\delta_{lat}(s)}\right|_{\substack{\theta \to \delta_{lon} \\ \psi \to \delta_{ped}}} = \frac{N^{\phi \quad \theta \quad \psi}_{\delta_{lat}\delta_{lon}\delta_{ped}}}{N^{\theta \quad \psi}_{\delta_{lon}\delta_{ped}}} \tag{8}$$

By comparing Eqs. (7) and (8) it can be seen that the roll frequency response will generally be different depending on whether or not pitch and yaw are constrained. Also, although Eq. (8) is a single-input single-output (SISO) transfer function, it does also reflect the overall MIMO nature of the helicopter response.

### Numerical calculation of multi-loop transfer functions

This section describes three related techniques to perform numerically, rather than symbolically, the manipulations required to obtain the multi-loop transfer functions.

**1. State-space approach**
The first technique consists of converting to pole/zero form the state space model corresponding to the desired inner loop control scheme. For the roll transfer function scheme of Fig. 1, and the specific arrangement of the $\mathbf{x}(t)$ and $\mathbf{u}(t)$ vectors used in this study, it is

$$\begin{aligned} \dot{\mathbf{x}}(t) &= A_{SS}\mathbf{x}(t) + B_{SS}\mathbf{u}(t) && (9) \\ &= A_{SS}\mathbf{x}(t) + B_{SS}(\mathbf{u}_1(t) + \mathbf{u}_2(t)) \\ &= (A_{SS} - B_{SS}K)\mathbf{x}(t) + B_{SS}\mathbf{u}_2(t) \\ &= A_{SScl}\mathbf{x}(t) + B_{SS}\mathbf{u}_2(t) && (10) \end{aligned}$$

where: $A_{SS}$ and $B_{SS}$ are the state and control matrices of the linearized system in state space form; $\mathbf{u}_1(t)$ is the pilot (or flight control system) input needed to close the pitch and yaw attitude loops, with $\mathbf{u}_1(t) = -K\mathbf{x}(t)$ and $K$ a matrix with all its elements to zero except for $K_{8,2} = Y_\theta$ and $K_{9,4} = Y_\psi$ (assuming $Y_\theta, Y_\psi$ = constant). Setting $Y_\theta$ and $Y_\psi$ to large (arbitrary) numbers implements the limit process indicated in Eq. (8). Then, the poles of the constrained transfer function are the eigenvalues of $A_{SScl}$. The zeros are the transmission zeros of the system composed of Eq. (10), an output row matrix $C$ with all its elements equal to zero except for that corresponding to $\phi$ (in the present study, $C_7$), and a zero matrix $D$ (in the present study $D$ is a scalar). These transmission zeros can be computed as shown, for example, in Ref. [8]. This technique is the easiest to set up because it is based on customary control system design tools. However, numerical overflow problems may arise if there are many feedback elements.

**2. Numerical calculation of coupling numerators**
The second technique is based on starting from Eq. (9) and taking the Laplace Transform of both sides:

$$\underbrace{(sI - A_{ss})}_{=A(s)}\mathbf{X}(s) = \underbrace{B_{ss}}_{=B}\mathbf{U}(s) \tag{11}$$

The $A(s)$ matrix only has polynomial terms on the diagonal, and $B$ has no polynomial terms at all. Computing

each of the $N$-terms in Eq. (6) corresponds to solving numerically the following generalized eigenvalue problem

$$A_B\mathbf{x} = \lambda E\mathbf{x} \tag{12}$$

where $A_B$ is the $A_{ss}$ matrix with the required number of its columns replaced by the appropriate columns of $B_{ss}$, and $E$ is essentially an identity matrix, except that the ones on the diagonal corresponding to the columns of $B_{ss}$ inserted in $A_{ss}$ are replaced by zeros. For example, consider a simple 3 by 3 $A_{ss}$ matrix. Then the system matrix $A(s)$ becomes

$$A(s) = \begin{bmatrix} s-a_{11} & -a_{12} & -a_{13} \\ a_{21} & s-a_{22} & -a_{23} \\ a_{31} & -a_{32} & s-a_{33} \end{bmatrix} \tag{13}$$

Assume now that we are interested in solving Eq. (11) for the open loop transfer function from the input $u_1(s)$ (first element of $\mathbf{U}(s)$) to the output $x_1(s)$ (first element of $\mathbf{X}(s)$). The transfer function will be

$$\frac{x_1(s)}{u_1(s)} = \frac{N_{x_1}^{u_1}(s)}{\Delta(s)} \tag{14}$$

where

$$N_{x_1}^{u_1}(s) = \begin{vmatrix} b_{11} & -a_{12} & -a_{13} \\ b_{21} & s-a_{22} & -a_{23} \\ b_{31} & -a_{32} & s-a_{33} \end{vmatrix} \tag{15}$$

The zeros of the transfer function are the values of $s$ such that $N_{x_1}^{u_1}(s) = 0$. These are the solutions of the following generalized eigenvalue problem:

$$\left( \begin{bmatrix} b_{11} & -a_{12} & -a_{13} \\ b_{21} & -a_{22} & -a_{23} \\ b_{31} & -a_{32} & -a_{33} \end{bmatrix} - s \begin{bmatrix} 0 & 0 & 0 \\ 0 & 1 & 0 \\ 0 & 0 & 1 \end{bmatrix} \right) \begin{Bmatrix} x_1 \\ x_2 \\ x_3 \end{Bmatrix} = \mathbf{0} \tag{16}$$

or, equivalently

$$\begin{bmatrix} b_{11} & -a_{12} & -a_{13} \\ b_{21} & -a_{22} & -a_{23} \\ b_{31} & -a_{32} & -a_{33} \end{bmatrix} \begin{Bmatrix} x_1 \\ x_2 \\ x_3 \end{Bmatrix} = s \begin{bmatrix} 0 & 0 & 0 \\ 0 & 1 & 0 \\ 0 & 0 & 1 \end{bmatrix} \begin{Bmatrix} x_1 \\ x_2 \\ x_3 \end{Bmatrix} \tag{17}$$

which is in the form of Eq. (12).

In the present study, the poles of the transfer function are either the zeros of the open loop characteristic polynomial $\Delta$, or the zeros of some coupling numerator like $N_{\delta_{lon}\delta_{ped}}^{\theta\ \ \psi}$ in Eq. (8), which can then be computed as just shown.

To complete the calculation it is necessary to compute the transfer function gain, i.e., the constant $K$ in the pole-zero form of the transfer function, that is

$$\frac{x_1(s)}{u_1(s)} = K\frac{(s-z_1)(s-z_2)}{(s-p_1)(s-p_2)(s-p_3)} \tag{18}$$

Where the $z$'s and the $p$'s are, respectively, the zeros and the poles of the transfer function. If the denominator of the transfer function is $\Delta$, then $K$ is only determined by the numerator, and can be calculated as follows. The determinant $N_{x_1}^{u_1}(s)$ is a polynomial in $s$ that can be written as:

$$N_{x_1}^{u_1}(s) = K(s-s_1)(s-s_2) \tag{19}$$

where $s_1$ and $s_2$ are the eigenvalues. Consider now an arbitrary value $s_0$ different from any of the eigenvalues. Then

$$K = \frac{N_{x_1}^{u_1}(s_0)}{(s_0-s_1)(s_0-s_2)} \tag{20}$$

or, for a general case with $n$ eigenvalues,

$$K = \frac{N_{x_1}^{u_1}(s_0)}{\prod_{i=1}^{n}(s_0-s_i)} \tag{21}$$

with $s_0 \neq s_i, i = 1, \ldots, N$. If the denominator of the transfer function is not $\Delta$, but some numerator like $N_{\delta_{lon}\delta_{ped}}^{\theta\ \ \psi}$ in Eq. (8), then there will be a constant $K_{num}$ for the numerator, and another $K_{den}$ for the denominator, each computed individually as just shown. Then it will be $K = K_{num}/K_{den}$. Compared with the state-space approach, this technique is slightly more complicated to set up, but is less subject to numerical problems and is equally efficient.

### 3. Coprime factorization

The third technique is based on computing a left coprime factorization [10] of the matrix transfer function corresponding to Eq. (10):

$$P(s)D^{-1}(s) = C(A_{ss} - B_{ss}K - sI)B_{ss} + D_{ss} \tag{22}$$

where $C$ is the identity matrix and $D_{ss} = 0$. In this study, $B_{ss}$ is really only the column of the true $B_{ss}$ matrix corresponding to the lateral cyclic input, i.e., the first column of $B_{ss}$. Then $D^{-1}(s)$ is the denominator of all the transfer functions from the desired input, and $P(s)$ is a vector, each element of which is the numerator of the transfer function corresponding to the desired output (or state). Both $P(s)$ and $D(s)$ contain polynomials that must be subsequently factored out to obtain, respectively, zeros and poles of the transfer function.

The individual coupling numerators can be obtained by setting equal to zero appropriate combinations of gains, i.e., of elements of the matrix $K$. For example, consider the transfer function

$$\left.\frac{\phi}{\delta_{lat}}\right|_{\substack{\theta \to \delta_{lon} \\ \psi \to \delta_{ped}}} = \frac{N_{\delta_{lat}}^{\phi} + Y_\theta N_{\delta_{lat}\delta_{lon}}^{\phi\ \theta} + Y_\psi N_{\delta_{lat}\delta_{ped}}^{\phi\ \psi} + Y_\theta Y_\psi N_{\delta_{lat}\delta_{lon}\delta_{ped}}^{\phi\ \theta\ \psi}}{\Delta + Y_\theta N_{\delta_{lon}}^{\theta} + Y_\psi N_{\delta_{ped}}^{\psi} + Y_\theta Y_\psi N_{\delta_{lon}\delta_{ped}}^{\theta\ \psi}}$$

(Eq. (6) repeated)

and let $Y_\theta = K_{8,2} = 0$ and $Y_\psi = K_{9,4} = 0$. Then from Eq. (22):

$$\frac{p(s)}{d(s)} = \frac{N^{\phi}_{\delta_{lat}}}{\Delta} \tag{23}$$

(where $p(s)$ and $d(s)$ are the appropriate elements of $P(s)$ and $D(s)$), and $N^{\phi}_{\delta_{lat}}$ and $\Delta$ can be obtained. Next, set $Y_\theta$ to some arbitrary constant value $Y_1$ and let still $Y_\psi = 0$. Equation (6) then simplifies to

$$\left.\frac{\phi}{\delta_{lat}}\right|_{\substack{\theta \to \delta_{lon} \\ \psi \to \delta_{ped}}} = \frac{p(s)}{d(s)} = \frac{N^{\phi}_{\delta_{lat}} + Y_1 N^{\phi\ \theta}_{\delta_{lat}\delta_{lon}}}{\Delta + Y_1 N^{\theta}_{\delta_{lon}}} \tag{24}$$

from which:

$$N^{\phi\ \theta}_{\delta_{lat}\delta_{lon}}(s) = \frac{1}{Y_1}\left[p(s) - N^{\phi}_{\delta_{lat}}(s)\right] \tag{25}$$

$$N^{\theta}_{\delta_{lon}}(s) = \frac{1}{Y_1}\left[d(s) - \Delta(s)\right] \tag{26}$$

Next, set $Y_\psi$ to some arbitrary constant value while letting $Y_\theta = 0$, to obtain $N^{\phi\ \psi}_{\delta_{lat}\delta_{ped}}$ and $N^{\psi}_{\delta_{ped}}$. Finally, set both $Y_\psi$ and $Y_\theta$ to some arbitrary constant value, and complete the calculations by obtaining $N^{\phi\ \theta\ \psi}_{\delta_{lat}\delta_{lon}\delta_{ped}}$ and $N^{\theta\ \psi}_{\delta_{lon}\delta_{ped}}$ (all the other coupling numerators necessary for this last step will be available at this point).

This technique is easy to set up for small numbers of inputs and outputs, thanks to the availability of public domain software (SLICOT library) that can perform numerically the coprime factorization for systems of arbitrary size. However, it can become cumbersome to apply if there are many feedback loops.

### Simulation model

The simulation model used in this study is a blade element-type, coupled-rotor fuselage model. The blades are modeled as flexible beams undergoing coupled flap-lag-torsion deformations. The rotor equations of motion are discretized using finite elements, and a modal coordinate transformation is used to reduce the number of rotor degrees of freedom. Three modes are retained in the present study, namely, rigid body flap and lag, and elastic torsion. The extended momentum theory of Keller and Curtiss is used to model the main rotor inflow. A one-state dynamic inflow model is used for the tail rotor. Quasi-steady stall and compressibility effects are introduced through look-up tables of airfoil aerodynamic coefficients. The rigid body motion of the fuselage is described through nonlinear Euler equations. The aerodynamic characteristics of the fuselage and of the empennage are described by look-up tables of aerodynamic coefficients. The trim procedure simulates free flight, and simultaneously enforces overall force and moment equilibrium on the aircraft, and the periodicity of the steady state motion of the rotor. The state space linearized model is obtain by perturbing numerically the equations of motion about this trimmed position.

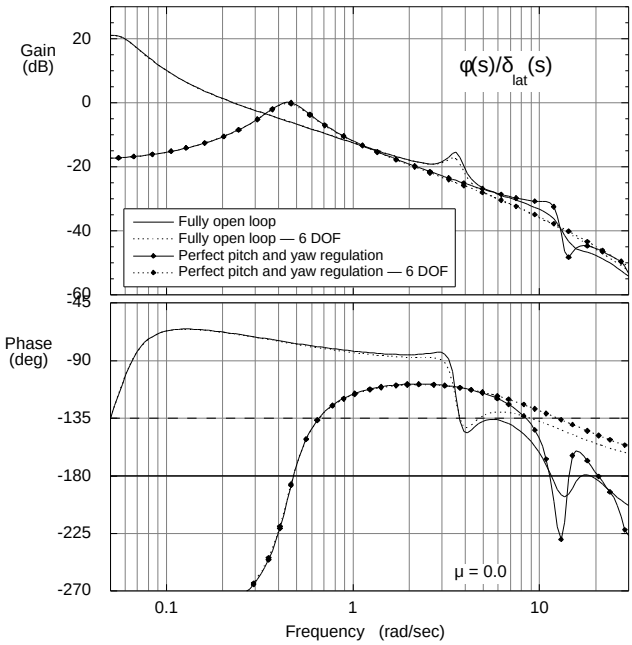


Figure 2: Roll frequency responses in hover.

### Results

The results presented in this section refer to a configuration very similar to the Eurocopter BO-105, at a hover $C_T/\sigma = 0.07$. The matrix of test cases was composed of:

1. Straight flight conditions, with speeds ranging from $V = 0$ to $V = 150$ kts, corresponding to advance ratios from $\mu = 0$ to $\mu \approx 0.36$.

2. Coordinated, level, right-handed, steady turns, with advance ratio $\mu = 0.2$, corresponding to $V = 84$ kts, and load factors from $n_T = 0$ to $n_T = 1.8$ (the highest value for which it was possible to trim the helicopter in the turn).

3. Coordinated, right- and left-handed, steady turns, with advance ratio $\mu = 0.2$, corresponding to $V = 84$ kts, flight path angles $\gamma = -20^o$ (i.e., descending turns), and load factors from $n_T = 0$ to $n_T = 1.8$ (also the highest value for which it was possible to trim the helicopter in the turn).

All the results were calculated using the state space approach previously described. For comparison, several results were also calculated with the numerical coupling numerator technique and with coprime factorizations. In all cases, the results obtained with the three methods were identical.

**Frequency response and bandwidth**

Figures 2 through 4 show the roll frequency response $\phi(s)/\theta_{1c}$. Each figure contains four curves, corresponding to: (i) the fully open loop system, i.e., the system with the pitch and yaw loops open; (ii) same as (i), but

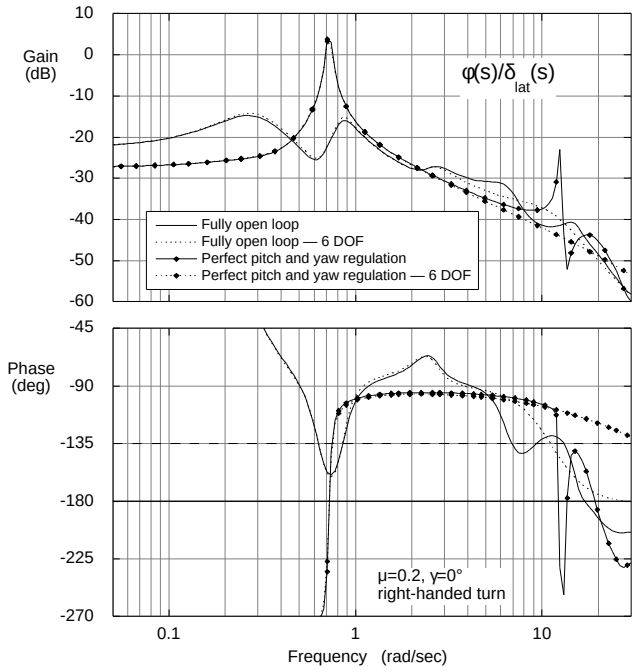


Figure 3: Roll frequency responses in steady turning flight.

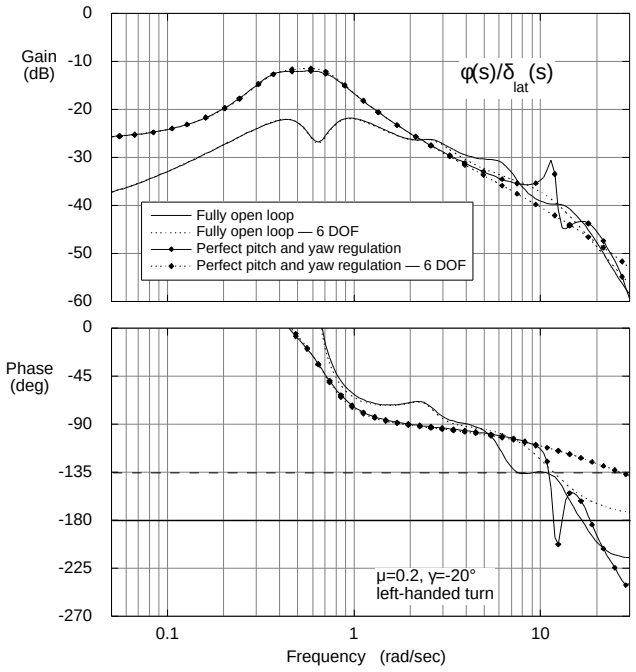


Figure 4: Roll frequency responses in descending steady turning flight.

for a reduced order, 6-DOF system obtained using static condensation; (iii) the system with perfect pitch and yaw regulation, i.e., with the pitch and yaw loops closed with infinite gain; and (iv) same as (iii), but for the reduced order, 6-DOF system.

Figure 2 refers to the hover case. The effect of the coupled rotor-body modes can be clearly seen in the range of frequencies between 1-2 and 20-30 rad/sec, which determine the bandwidth parameters. The dip in the phase plot at the frequency of about 13 rad/sec is associated with the regressive lag mode (for a fundamental lag frequency of $\omega_{L1} = 0.7$/rev and a rotor speed of $\Omega = 44.4$ rad/sec, the frequency $1 - \omega_{L1} = 13.3$ rad/sec). Perfect off-axis regulation does not significantly change the frequency, but makes the dip much more pronounced. The effect of the rotor modes is completely missed by the approximate, 6-DOF models, which smoothly approach the high frequency asymptotic phase value of $-180^o$. In general, these simplified models are not reliable for the calculation of the bandwidth of a helicopter configuration like this, with rotor modes so close to the phase crossover frequency $\omega_{180}$. Reduced order models with at least one or two rotor modes might be acceptable, but such models were not explored in the present study.

Using the ADS-33 definitions [11], the phase and gain bandwidths of the fully open loop system are 3.7 and 6.8 rad/sec, respectively. With perfect pitch and yaw regulation, the corresponding figures become 8.5 and 4.0 rad/sec. Therefore, the unconstrained system is phase limited, whereas the constrained system is gain limited. The bandwidths for the reduced order models are 3.7 and 12.5 rad/sec respectively (they coincide with the phase bandwidth because the gain bandwidth is undefined for a 6-DOF model).

Figure 3 refers to a coordinated, level, right-handed, steady turn, at an advance ratio $\mu = 0.2$ and load factor $n_T = 1.8$. In this case, the phase dip at the regressive lag mode frequency is essentially unnoticeable for the fully open loop case, but it becomes a very sharp notch with perfect off-axis regulation. Again, using the ADS-33 definitions, the phase and gain bandwidths of the fully open loop system are 6.9 and 8.2 rad/sec, respectively. With perfect pitch and yaw regulation, the corresponding figures become 12.0 and 1.2 rad/sec. Therefore, again the unconstrained system is phase limited, whereas the constrained system is gain limited. However, the significance of the gain bandwidth value of 1.2 rad/sec for the constrained system is questionable. In fact, such a low value is caused by the rapid variations of the gain curve around the $\omega_{180}$ frequency. Very different values would be obtained by slightly increasing or decreasing $\omega_{180}$, and common sense suggests that these variations would not really affect the handling qualities of the helicopter. ADS-33 does not currently offer guidance on how to handle strong nonlinearities of the gain and phase curves in bandwidth calculations, as it does for phase delay calculations. The bandwidth values for the 6-DOF approximate models are 11.1 rad/sec for the unconstrained system, and an unrealistically high 36.3 rad/sec for the constrained system.

The same general features can be seen in Fig. 4 for a descending turning flight case. Again, the advance ratio

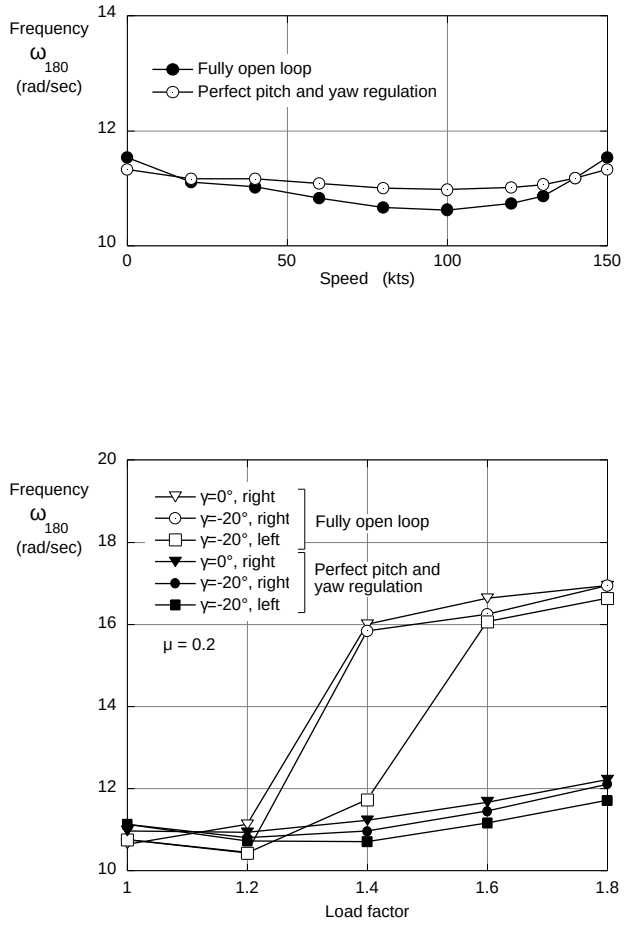


Figure 5: Phase crossover frequencies $\omega_{180}$ for straight flight (top) and steady turns (bottom).

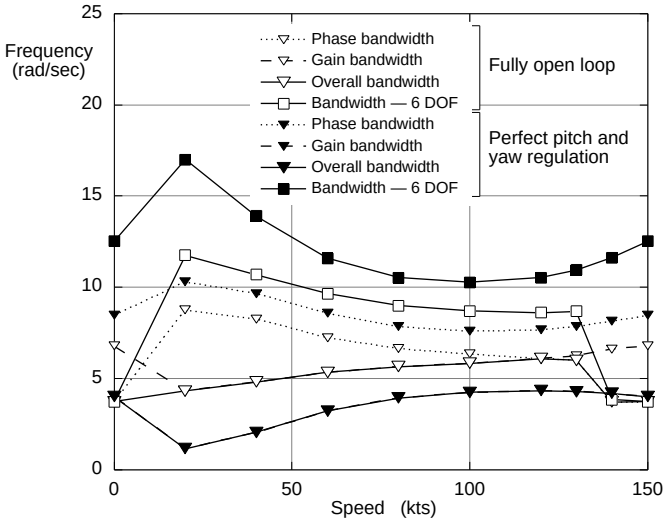


Figure 6: Roll bandwidth in straight flight according to ADS-33.

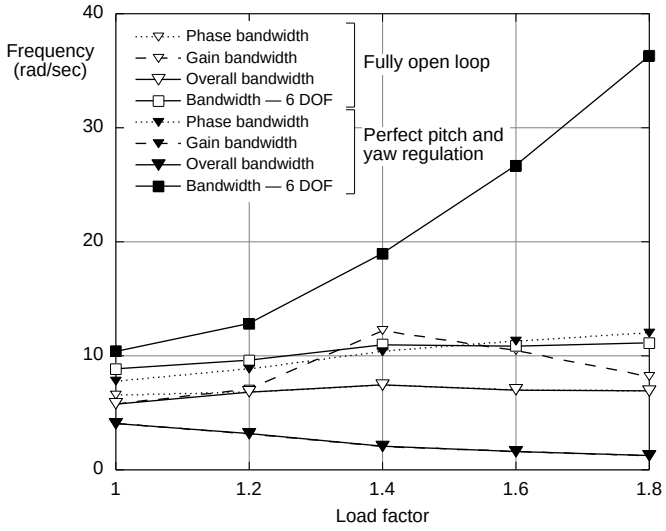


Figure 7: Roll bandwidth in right-handed, steady, level turns, according to ADS-33; $\mu = 0.2$.

is $\mu = 0.2$ and the load factor $n_T = 1.8$, but the flight path angle is $\gamma = -20^o$ and the turn is left-handed. The phase and gain bandwidths of the fully open loop system are 7.6 and 8.6 rad/sec, respectively. With perfect pitch and yaw regulation, the corresponding figures become 11.1 and 2.3 rad/sec, i.e., the system goes from phase- to gain-limited. As in the previous case, the very low value of the gain bandwidth for the constrained case is related to strong nonlinearities of the gain and phase curves around the frequency of the regressive lag mode, and its practical significance is questionable. In fact, the penalty for low gain bandwidth in ADS-33 is intended to prevent gain curves with flat regions, which tend to result in configurations that are prone to Pilot-Induced Oscillations (PIO) [12]. Instead, not only do the gain curves in Figs. 3 and 4 not show flat regions, but they have the desired $1/s$ behavior over large portions of the important 1-10 rad/sec frequency band.

Figure 5 summarizes the phase crossover frequencies $\omega_{180}$ for all flight conditions. The top plot shows the variation with speed for the straight flight conditions. The values $\omega_{180}$ do not vary significantly with speed, and the effects of perfect pitch and yaw regulation are also modest. The corresponding values for turning flight are shown in the bottom plot as a function of load factor. The behavior for the unconstrained cases is primarily driven by the changes in shape of the dip of the phase curve around the regressive lag mode frequency. There are abrupt changes in $\omega_{180}$ between $n_T$=1.2 and 1.4 for the level turns and the right-handed descending turns, and between 1.4 and 1.6 for the descending left-handed turns. Outside these regions, the variations are small. The variations with $n_T$ are always small for the constrained cases, because the frequency of the phase dip changes little.

The roll bandwidths according to ADS-33 [11] are pre-

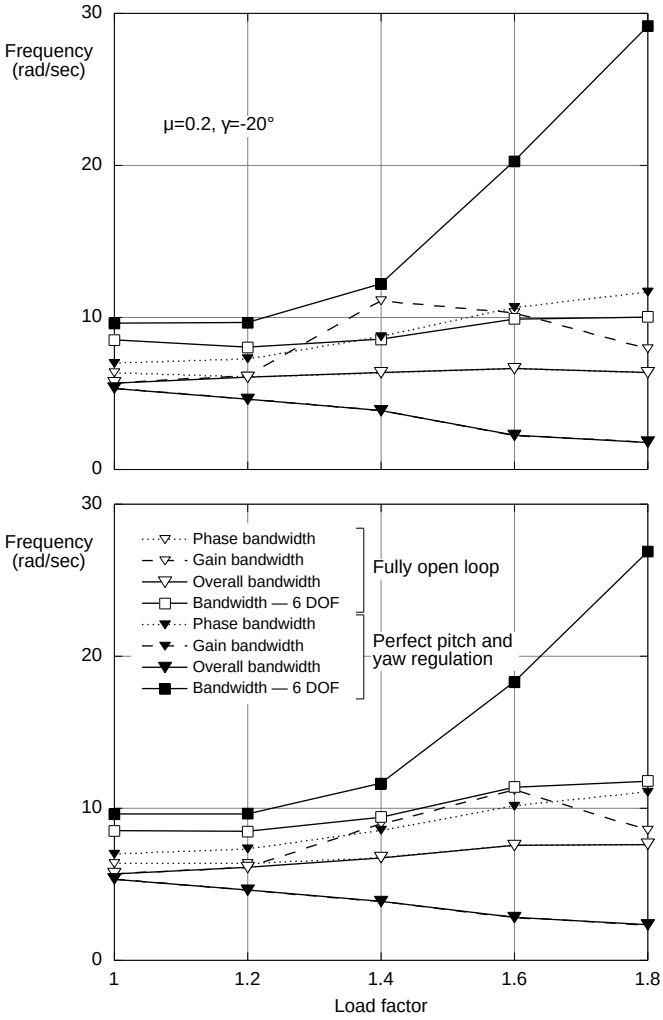


Figure 8: Roll bandwidth in steady, right-handed (top) or left-handed (bottom), descending turns, according to ADS-33.

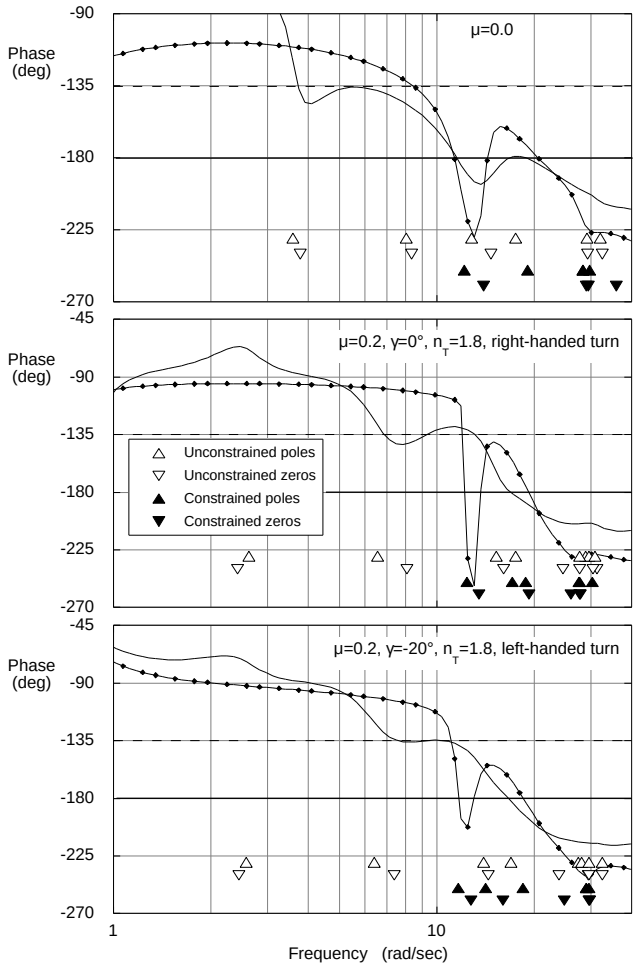


Figure 9: Phases of roll frequency responses (detail), poles and zeros; "Unconstrained" implies fully open loop, "Constrained" implies perfect pitch and yaw regulation.

sented in Figs. 6 through 8 for the straight flight, level turns, and descending turns, respectively. Each plot shows gain, phase, and overall bandwidth for the full and reduced order models, and for the unconstrained and constrained cases. Except at hover and above 140 kts, the system is gain limited in straight flight, as shown in Fig. 6. Perfect pitch and yaw regulation reduces the bandwidth at almost all speeds. The constrained system is also gain limited. The reduced order models greatly overpredict bandwidth at almost all speeds for the unconstrained and, especially, the unconstrained configurations. The open loop system is phase limited in level, Fig. 7, and descending turns, Fig. 8, for most values of load factor, with the bandwidth changing little with load factor. On the other hand, the constrained system is typically gain limited, both in level and descending turns. The bandwidth decreases slowly with load factor.

To better understand the changes in the phase curves that play such a key role in driving the bandwidth, Fig. 9 shows details of the phase plots for the roll frequency responses. Poles and zeros in the frequency ranges of interest are also shown for both the fully open loop case and the case with perfect pitch and yaw regulation. The top plot refers to the hover case. For the fully open loop case, there are two pole/zero pairs below the $\omega_{180}$ frequency, tentatively identified as a pitch short period mode (slightly below 4 rad/sec) and a flap regressive mode (at around 8 rad/sec). Perfect pitch and yaw regulation removes these two dipoles. Between 10 and 20 rad/sec there are two poles and one zero, collectively associated with the regressive lag mode and the roll damping mode. They are present for both the unconstrained and the constrained case. In the latter, a slight change in relative position and, especially, a reduction in damping cause a deeper dip in the phase curve. The same general features are evident in the phase plot for the level turn (middle plot) and the descending turn (bottom plot). In other words, the changes in frequency and damping of these two poles and one zero, and their relative separation, are the primary cause for all the nonlinearities in the gain and phase curves, and therefore for all the changes in bandwidth introduced by perfect pitch and yaw regulation.

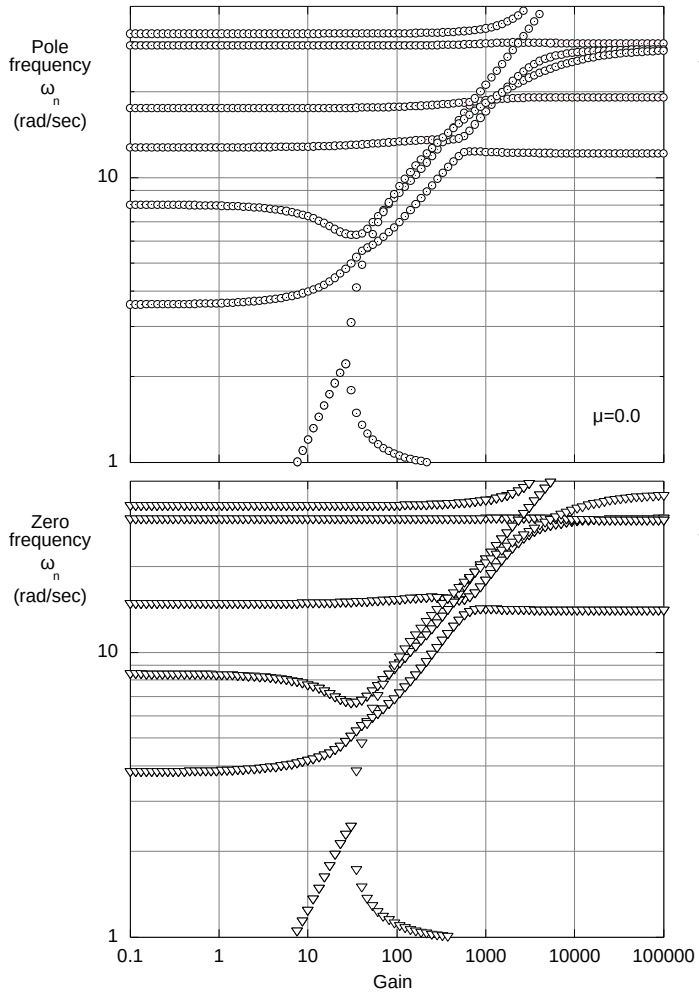


Figure 10: Frequency of selected poles and zeros for increasing gain; hover.

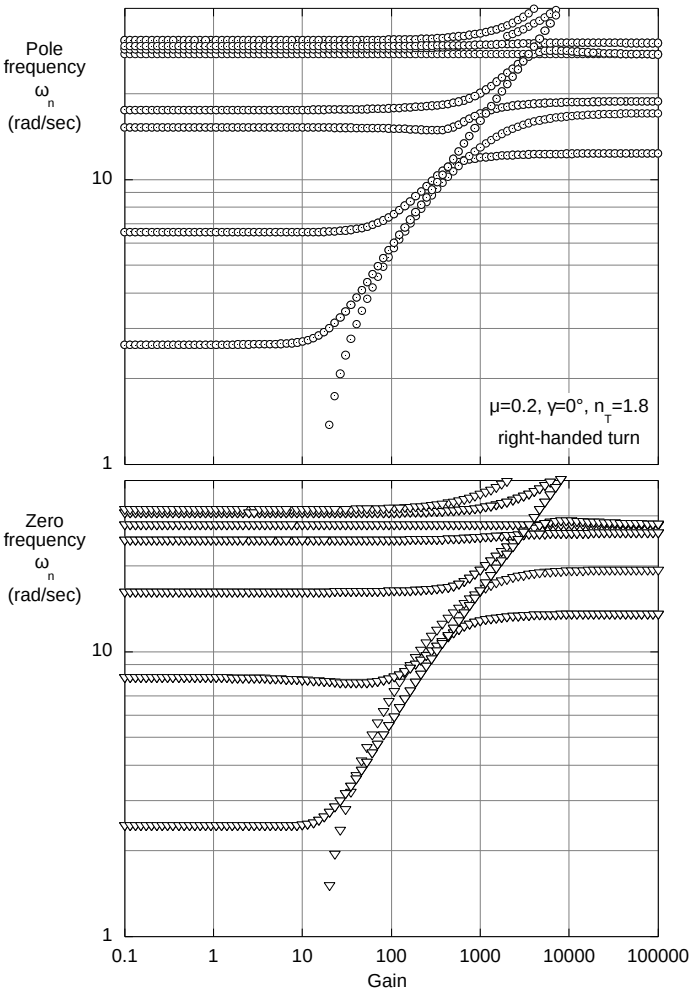


Figure 11: Frequency of selected poles and zeros for increasing gain; steady level turn.

To further understand these changes Figs. 10 through 12 show the frequency of selected poles and zeros for increasing gain $K$ for the three flight conditions previously considered. The units for $K$ are degrees of swashplate input per radian of attitude angle (therefore, to obtain the values of $K$ in deg/deg, the numbers on the $x$-axis must be divided by 57.3). Figure 10 shows the hover results. Although the effects of off-axis loop closure can be seen for as low as $K = 1$, most of the effects are concentrated in the range $10 < K < 1000$ deg/rad, corresponding to approximately $0.2 < K < 18$ deg/deg. The frequency of some poles and zeros continues to change for higher $K$, and it becomes constant only for gains 100 times higher. Qualitatively similar results can be seen for the level turn case, Fig. 11, and the descending turn case, Fig. 12. In other words, although significant changes in the frequencies of poles and zeros occur for realistic values of the gains, to achieve "perfect" regulation the gains need be so high that they are probably impossible to achieve. Therefore, while the assumption of perfect regulation is convenient because it is intuitively clear and because it leads to a simple mathematical treatment, the results obtained by making this assumption should be examined critically, at least for bandwidth calculations. The configuration used in this study appears to be very sensitive to the precise position of poles and zeros between $\omega_{180}$ and $2\omega_{180}$. As a consequence, the bandwidth results obtained using the assumption of perfect regulation are probably not realistic.

**Damping of the regressive lag mode**

Considering now the effects of pilot regulation on aeroelastic stability, Figs. 13, 14, and 15 show selected poles and zeros in steady, descending, and left-handed turn, respectively. In all figures, the circle marked "RLM" shows poles and zeros of the regressive lag mode. In hover, the damping ratio of the regressive lag mode goes from an unconstrained value of $\zeta = 0.238$ to a constrained value of $\zeta = 0.111$, for a reduction of 53%. The situation is worse for the right handed level turn, Fig. 14, where the mode almost becomes neutrally stable, with $\zeta$ going from 0.122 to 0.007. A substantial loss of damping can also be observed for the descending left turn case, Fig. 15. Here, the damping decreases from $\zeta = 0.172$ to $\zeta = 0.041$, for a loss of 76%. In other words, the actions by the pilot to perfectly cancel out pitch and yaw from roll appear to reduce the damping of the regressive

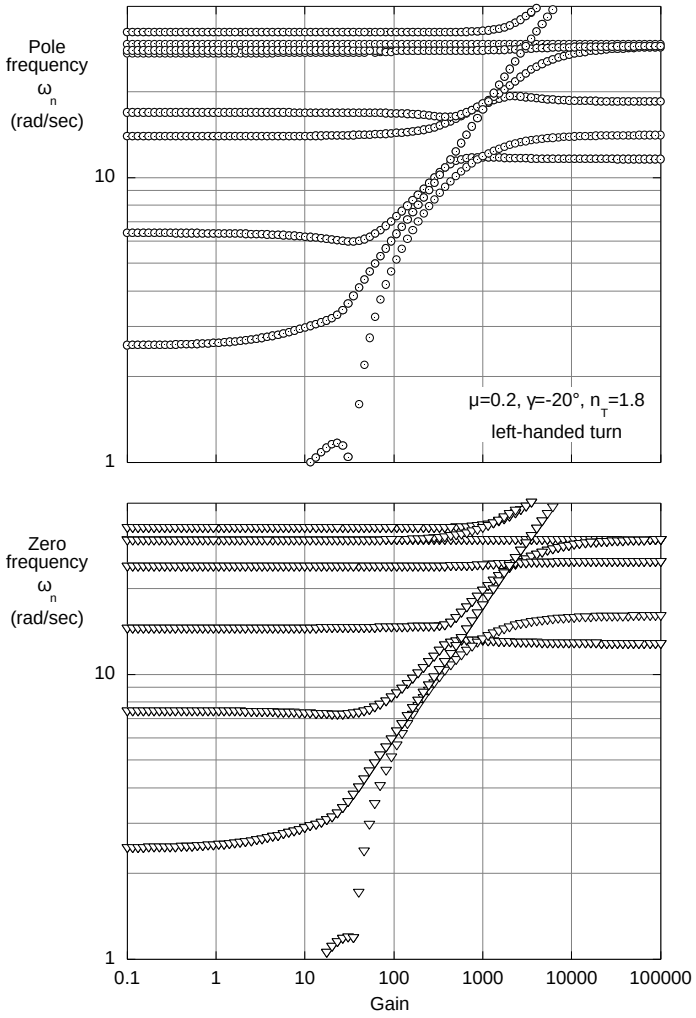


Figure 12: Frequency of selected poles and zeros for increasing gain; steady descending turn.

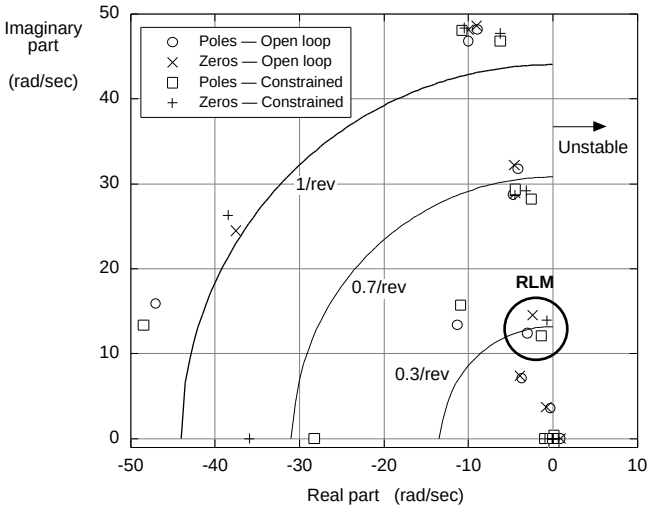


Figure 13: Selected poles and zeros in hover; "Unconstrained": fully open loop, "Constrained": perfect pitch and yaw regulation; "RLM": regressive lag mode.

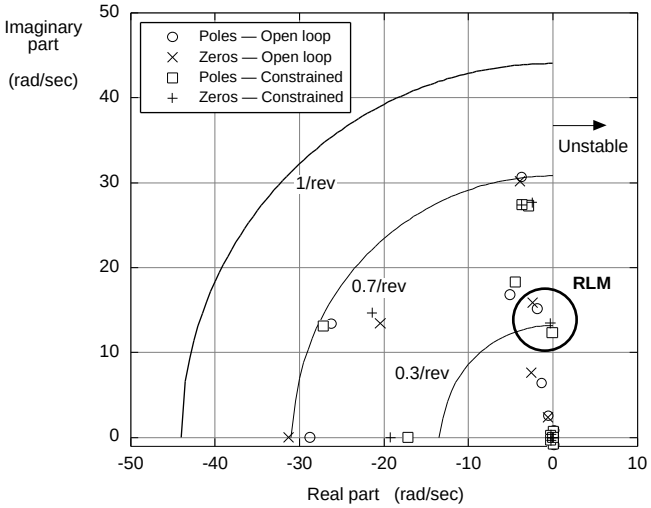


Figure 14: Selected poles and zeros in steady, level, right-handed turn, $\mu = 0.2$, $n_T = 1.8$; "Unconstrained": fully open loop, "Constrained": perfect pitch and yaw regulation; "RLM": regressive lag mode.

lag mode, thereby triggering a sort of pilot-rotor coupling. This coupling appears to be similar to Aircraft-Pilot Coupling (APC), which is another designation for Pilot-Induced Oscillations (PIO), in the sense that it is a pilot-in-the-loop phenomenon, and therefore it disappears if the pilot interrupts the off-axis canceling action.

To determine to what extent the previous considerations are influenced by the actual values of the gain, Fig. 16 shows frequency and damping of regressive lag poles and zeros as a function of gain $K$ for the three flight conditions previously considered. As in the bandwidth case, the figure shows that the assumption of "perfect" regulation does not necessarily provide a precise description, because the corresponding gains are unrealistically high. On the other hand, the figure also shows that even for realistic values of $K$ some loss of damping does occur, and the extent of the loss increases with gain. There is only anecdotal evidence of loss of rotor damping actually occurring during maneuvers for hingeless and bearingless rotor helicopters, but no documented cases. Therefore, it cannot be stated conclusively that pilot-rotor coupling is a real effect rather than a mathematical artifact. If pilot-rotor coupling did indeed exist, an interesting consequence would be that the lag mode damping would not be an intrinsic property of a rotor system, but it would also depend to some extent on the individual pilot, and for a given pilot, on the piloting strategy (i.e., on the decision on how tightly to close the off-axis response attitude loops).

## Conclusions

The paper presented the derivation of three techniques for the numerical calculation of multi-loop transfer functions. Because these techniques do not require symbolic manipulations, they allow the introduction of rotor dynamics and other higher-order effects in the calculation of the transfer functions. The techniques were applied to the study of the roll dynamics of a hingeless rotor helicopter with the pitch and yaw response eliminated by assuming infinitely tight feedback loop. Both straight

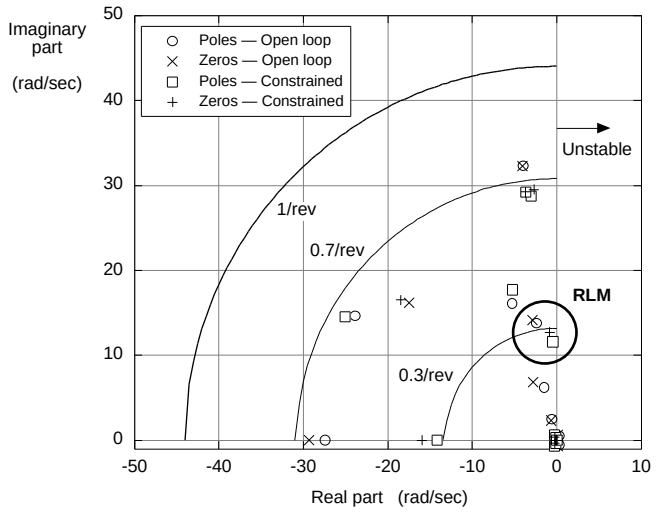


Figure 15: Selected poles and zeros in steady, descending, left-handed turn, $\mu = 0.2$, $\gamma = -20^o$, $n_T = 1.8$; "Unconstrained": fully open loop, "Constrained": perfect pitch and yaw regulation; "RLM": regressive lag mode.

and turning flight conditions were considered. The helicopter chosen for the study has a hingeless rotor system, which induces strong coupling among the rigid body degrees of freedom, and between rotor and fuselage degrees of freedom.

The key conclusion of the present study are:

1. The combination of perfect pilot regulation of off-axis response and low frequency rotor modes can have repercussion on handling qualities. Following the definitions of the ADS-33 handling qualities specification, significant bandwidth changes can be observed, and the constrained system typically switches from phase- to gain-limited. However, the bandwidth changes are caused by the nonlinearity of the gain and phase curves around the phase crossover frequency, and do not necessarily reflect the underlying philosophy of the specification. Therefore, their practical implications remain to be determined. Few, if any, of the effects on bandwidth of perfect regulation of pitch and roll can be captured with simplified, 6-DOF models.

2. The combination of perfect pilot regulation of off-axis response and low frequency rotor modes can negatively affect aeroelastic stability. For the configuration used in this study, the damping of the regressive lag mode drops substantially with perfect pitch and yaw regulation, both in straight and in turning flight. The possibility of destabilizing pilot-rotor coupling appears to exist.

3. The two previous conclusions are valid for a "perfect" regulation obtained assuming infinitely high gains in the off-axis response feedback loops. While this assumption is convenient and simple, it should be critically examined for every configuration. Most of the effects of perfect regulation on the bandwidth occur for gains so high that they could not be considered completely realistic. This is generally also true for the effects on aeroelastic stability, but some symptoms of pilot-rotor coupling do appear for realistic values of gains, so the phenomenon merits further study.

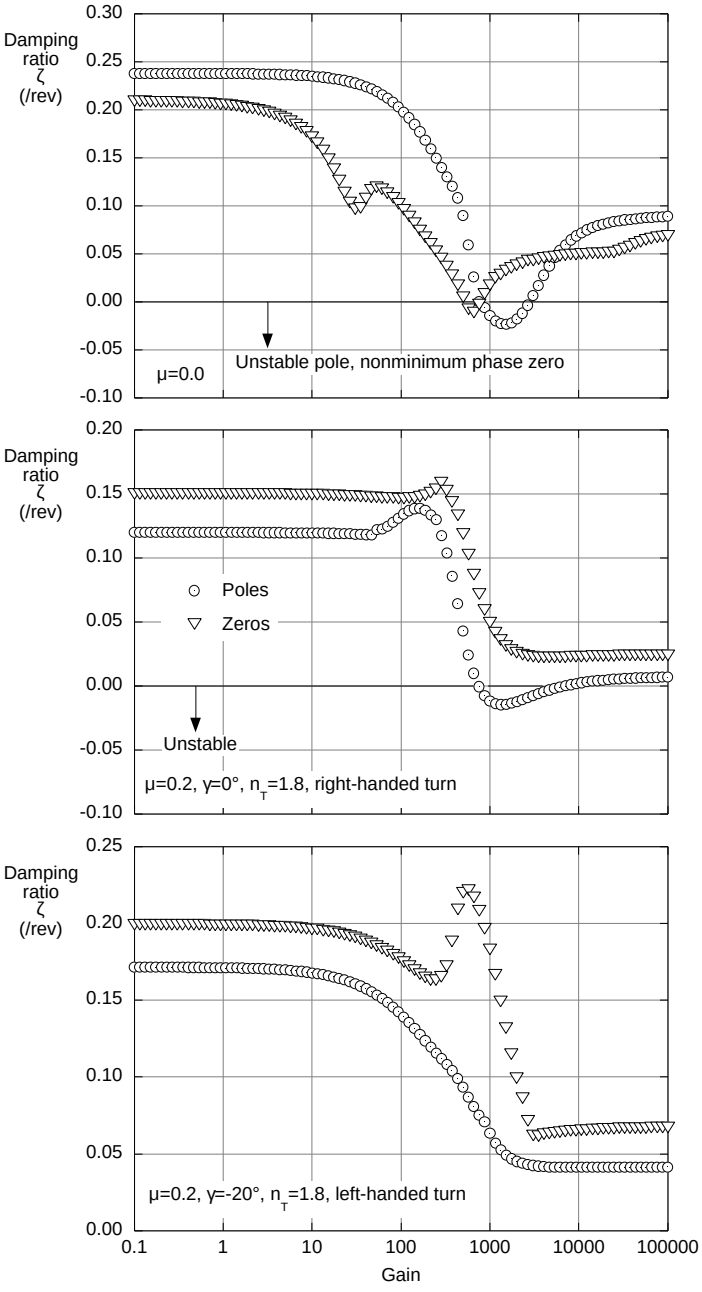


Figure 16: Frequency and damping of regressive lag poles and zeros for increasing gain.


### Acknowledgments

This research was supported by the National Rotorcraft Technology Center under the Rotorcraft Center of Excellence Program, Technical Monitor Dr. Y. Yu.

## References

[1]Padfield, G. D., *Helicopter Flight Dynamics: The Theory and Application of Flying Qualities and Simulation Modeling*, AIAA Education Series, Washington, DC, 1996, Chapter 5.

[2]McRuer, D., Ashkenas, I., and Graham, D., *Aircraft Dynamics and Automatic Control*, Princeton University Press, Princeton, NJ, 1973, Chapter 3.

[3]McRuer, D. T., and Krendel, E. S., "Mathematical Models of Human Pilot Behavior," AGARDograph No. 188, 1974.

[4]Heffley, R. K., "A Compilation and Analysis of Helicopter Handling Qualities Data—Volume Two: Data Analysis," NASA CR-3145, August 1979.

[5]Tischler, M. B., "Digital Control of Highly Augmented Combat Rotorcraft," NASA TM 88346, May 1987.

[6]Catapang, D. R., Tischler, M. B., and Biezad, D. J., "Robust Crossfeed Design for Hovering Rotorcraft," *International Journal of Control*, Vol. 4, No. 1, January 1994, pp. 161-180.

[7]Hess, R. A., "Coupling Numerators and Input-Pairing in Square Control Systems," *Journal of Guidance, Control, and Dynamics*, Vol. 26, No. 2, March-April 2003, pp. 367-369.

[8]Maciejowski, J. M., *Multivariable Feedback Design*, Addison-Wesley, 1989, Chapter 8.

[9]Misra, P., Van Dooren, P., and Varga, A., "Computation of Structural Invariants of Generalized State-space Systems," *Automatica*, Vol. 30, No. 12, 1994, pp. 1921-1936.

[10]Patel, R. V., "On Computing Matrix Fraction Descriptions and Canonical Forms of Linear Time-Invariant Systems," UMIST Control Systems Centre Report 489, 1980.

[11]Anonymous, "Handling Qualities Requirements for Military Rotorcraft", US Army Aviation and Missile Command, ADS-33E-PRF, 2000.

[12]Hoh, R. H., "Dynamic Requirements in the New Handling Qualities Specification for U.S. Military Rotorcraft," Royal Aeronautical Society's Conference on Helicopter Handling Qualities and Control, London, November 1988.


## Appendix
## Derivation of multi-loop transfer functions

This appendix summarizes the key points of the derivation of multi-loop transfer functions. The complete development can be found in Ref. [2].

Assume that the linearized equations of motion of the helicopter are written in Laplace Transform form as:

$$A(s)\mathbf{X}(s) = B(s)\mathbf{U}(s) \tag{27}$$

where $\mathbf{X}(s)$ is a vector of states and $\mathbf{U}(s)$ is a vector of controls. The system matrix $A(s)$ and the control matrix $B(s)$ are generally composed of polynomials in $s$ that result from Laplace transforming accelerations and rates (e.g., in straight and level flight, $\dot{q} \rightarrow s^2\theta(s)$, and $q \rightarrow s\theta(s)$) The solution of Eq. (27) can be obtained using Cramer's rule. For example, the transfer function from the input (or control) $\delta_1$ to the output $x_1$ is given by:

$$\frac{x_1(s)}{\delta_1(s)} = \frac{\begin{vmatrix} b_{11} & a_{12} & a_{13} \\ b_{21} & a_{22} & a_{23} \\ b_{31} & a_{32} & a_{33} \end{vmatrix}}{\begin{vmatrix} a_{11} & a_{12} & a_{13} \\ a_{21} & a_{22} & a_{23} \\ a_{31} & a_{32} & a_{33} \end{vmatrix}} = \frac{N^{x_1}_{\delta_1}}{\Delta} \tag{28}$$

where $\Delta$ is the determinant of the matrix $A(s)$, and $N^{x_i}_{\delta_j}$ is a short-hand notation to denote the determinant of the matrix obtained from the $A(s)$ matrix by replacing the $i$-th column of $A(s)$ with the $j$-th column of $B(s)$, that is:

$$N^{x_i \leftarrow \text{ input (control)}}_{\delta_j \leftarrow \text{ output (state)}}$$

The *closed-loop* transfer functions can be written in a general form as:

$$G_{CL}(s) = \frac{\text{effective numerator}}{\text{effective denominator}} \tag{29}$$

The details of the rules to form the "effective" numerator and denominator depend on the number of degrees of freedom explicitly manipulated or fed back, and the number of control deflections. For the system of Fig. 1, which has three degrees of freedom and three control deflections, the effective denominator is given by:

1. the open loop denominator $\Delta$,
2. plus the sum of all the feedback transfer functions, each one multiplied by the appropriate numerator,
3. plus the sum of all the feedback transfer functions taken two at a time, each pair multiplied by the appropriate coupling numerator.

For this case, the rule gives

$$\begin{aligned} \text{effective denominator} \quad &= \quad \Delta + Y_\theta N^\theta_{\delta_{lon}} \\ &\quad + Y_\psi N^\psi_{\delta_{ped}} + Y_\theta Y_\psi N^{\theta \quad \psi}_{\delta_{lon} \delta_{ped}} \end{aligned} \tag{30}$$

The effective numerator is given by:

1. The open loop numerator,
2. plus the sum of all the feedback transfer functions, each one multiplied by the appropriate coupling numerator,

3. plus the sum of all the feedback transfer functions taken two at a time, each pair multiplied by the appropriate type-two coupling numerator.

For this case, the rule gives

$$\begin{aligned}\text{effective numerator} \quad &= \quad N^{\phi}_{\delta_{lat}} + Y_\theta N^{\phi\ \theta}_{\delta_{lat}\delta_{lon}} \\ &+ Y_\psi N^{\phi\ \psi}_{\delta_{lat}\delta_{ped}} + Y_\theta Y_\psi N^{\phi\ \theta\ \psi}_{\delta_{lat}\delta_{lon}\delta_{ped}} \end{aligned} \tag{31}$$

Numerators, coupling numerators, and type-two coupling numerators are denoted by the letter $N$ and, respectively, one, two, and three subscript/superscript pairs. For coupling numerators with two and three subscript/superscript pairs, two and three columns of $A(s)$ are replaced by the same number of columns of $B(s)$.